First beam waist measurements in the final focus beam line at the KEK Accelerator Test Facility

Sha Bai,[1] Alexander Aryshev,[2] Philip Bambade,[2,3] Doug Mc Cormick,[4] Benoit Bolzon,[5] Jie Gao,[1] Toshiaki Tauchi,[2] and Feng Zhou[4]

[1]*IHEP, Beijing, China*
[2]*KEK, Tsukuba, Ibaraki, Japan*
[3]*LAL, Université Paris-Sud, CNRS/IN2P3, Orsay, France*
[4]*SLAC, California 94025, USA*
[5]*LAPP, Annecy, France*

(Received 8 January 2010; published 22 September 2010)

The ATF2 project is the final focus system prototype for the ILC and CLIC linear collider projects, with a purpose to reach a 37 nm vertical beam size at the interaction point using compact optics based on a novel scheme of local chromaticity correction. Construction of all components and installation were completed at the end of 2008. An initial commissioning phase followed in 2009, using larger than nominal β functions at the interaction point, corresponding to reduced demagnification factors in comparison to the design, to limit effects from higher-order optical aberrations and hence simplify beam tuning procedures while key instrumentation was being tested and calibrated. In this paper, first measurements of dispersion and Twiss parameters are presented based on scanning the beam during this period with a set of tungsten wires located just behind the interaction point, using two complementary analysis methods.

DOI: 10.1103/PhysRevSTAB.13.092804 PACS numbers: 29.27.Eg, 41.85.Ja

I. INTRODUCTION

ATF2 [1,2] is a test facility for ILC [3] and CLIC [4] type final focus systems based on local chromaticity correction [5]. It makes use of the low emittance beam extracted from the Accelerator Test Facility (ATF) damping ring, and aims to reach a final beam size of 37 nm at the optical focal point [hereafter referred to as interaction point (IP), by analogy to the linear collider collision point] after correcting for the effects of inaccuracies in magnet strengths and alignment. To measure such a small beam size at the IP, a ''Shintake'' monitor [6] based on colliding the beam with the interference pattern from lasers is used [7]. In addition, wire scanners with diameters 10 and 5 μm, respectively in tungsten and carbon, are placed 40 cm behind the IP to measure the beam sizes during initial tuning, with resolutions of about 2.5 and 1.25 μm. When these wire scanners were used, the waists in both planes were moved to the post-IP location by readjusting the currents of the final doublet QD0 and QF1 quadrupole magnets [8].

During the first commissioning in March 2009, a large β optics configuration was used at the IP, with 20 and 800 times the nominal values for β_x (0.08 m) and β_y (0.08 m), respectively. Sextupole magnets were turned off to reduce the sensitivity to misalignments. Starting in April 2009, β_y was reduced to 100 times the nominal value (0.01 m). Such optical configurations were used as key instrumentation was being tested and calibrated. Effects from higher-order optical aberrations being negligible with such large values of β [8], beam tuning procedures in the presence of imperfections were simpler and involved beam sizes at the post-IP wire scanner which were typically large enough to be resolved. The design beam parameters expected in a fully corrected system are shown in Table I for both the nominal optics and presently used large β configuration.

The first complete beam waist measurements at the ATF2 IP were done during the Spring commissioning in 2009. These measurements were used to provide first estimates of Twiss parameters at the IP and of the horizontal emittance, before implementing systematic optical corrections. The results obtained, using two analysis methods, are described in this paper.

The measurements consisted in varying the QD0 magnet current and recording horizontal and vertical beam sizes with the post-IP wire scanners. In the vicinity of the IP waists, the beam sizes σ_x and σ_y can be shown to depend on beam parameters and on the longitudinal displacement $\Delta f_{x,y}$ of each waist from the nominal location according to [9]

$$\sigma_{x,y}{}^2 = \varepsilon_{x,y}\beta_{x,y} + \frac{\varepsilon_{x,y}}{\beta_{x,y}}\Delta f_{x,y}{}^2, \tag{1}$$

TABLE I. Beam parameters with nominal and large β optics.

	Large β optics		Nominal β optics	
	Nominal IP	Wire scanner	Nominal IP	Wire scanner
β_x (cm)	8.0	9.90	0.4	0.495
β_y (cm)	1.0	1.84	0.01	0.0184
σ_x (μm)	12.7	14.1	2.80	3.15
σ_y (μm)	0.343	0.466	0.0343	0.0466
ε_x (nm)		2.0		
ε_y (pm)		12		

 © 2010 The American Physical Society

where $\beta_{x,y}$ and $\varepsilon_{x,y}$ are the horizontal and vertical β functions and emittances, respectively. By fitting parabolic dependencies to the measured data as a function of the QD0 magnet currents, the parameters in (1) could be determined. For both the emittance and β function to be determined simultaneously, it is essential to resolve the minimum beam size at the waist. This was the case in the horizontal but not in the vertical plane. For the latter, estimates of the β function could still be inferred from the second term in (1), without requiring the minimum beam size to be resolved, by using values for the emittance measured upstream, for example, after extraction from the damping ring or within the damping ring.

After briefly describing the post-IP wire scanners used at ATF2, the measurement results using the tungsten wires from two data sets collected in May 2009 are reported. We then describe the procedures to correct the measured data for dispersion and finite wire size, as well as the estimation of Twiss parameters and horizontal emittance. The results obtained were useful to provide first comparisons with the expected values in the optical configuration used. A few prospects towards the systematic implementation of the described methods during beam size minimization at the ATF2 IP are discussed in the last section.

II. POST-IP WIRE SCANNERS

A. Overview

The wire scanners installed behind the IP at ATF2 were assembled from two different similar systems used in the SLAC final focus test beam [10].

Three tungsten wires with 10 μm in diameter are strung on a 45° scanner located 40 cm behind the IP vertically, horizontally, and perpendicularly to the scanner, to measure the X and Y distributions and their correlation, respectively. This scanner, shown in the upper part of the schematic in Fig. 1, moves in steps of 1 μm (or 0.7 μm for the wires), in a range of about 24 mm, limited by two end switches. A vertical scanner placed 1.5 cm behind the 45° scanner is also shown in the lower part of the schematic. It has three carbon wires with 5 μm in diameter, one horizontal and the two others rotated by ± 1.3 degree. This scanner and its wires move in 100 nm steps, in a range of ± 3.0 mm and with maximum speed of 20 μm per second [11].

The bremsstrahlung photons produced when beam electrons interact in the wire material are measured in a Cherenkov detector [12] located further downstream, after a dipole magnet used to bend the beam towards the final dump.

B. Effect of wire width on the beam size measurement

The shape of the distribution of number of bremsstrahlung photons produced when the wire is scanned across the beam can be computed by folding the beam particle and wire material distributions, assumed to be, respectively, Gaussian and cylindrical [13]:

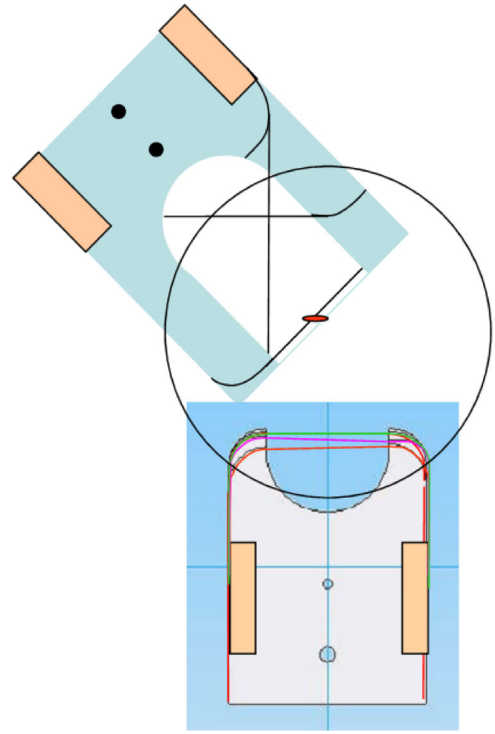

FIG. 1. Schematic of wire scanners installed behind the IP of ATF2.

$$f(a) = \int_{-d/2}^{d/2} 2\sqrt{\frac{d^2}{4} - x^2}\,\frac{1}{\sigma\sqrt{2\pi}}\,e^{-[(x-a)^2/2\sigma^2]}dx, \qquad (2)$$

where a is the offset between the centers of the two distributions, d is the wire diameter, and σ is the root mean square size of the beam particle distribution.

The result of fitting a Gaussian to the numerical computation in (2) is shown in the red curve in Fig. 2 for the case

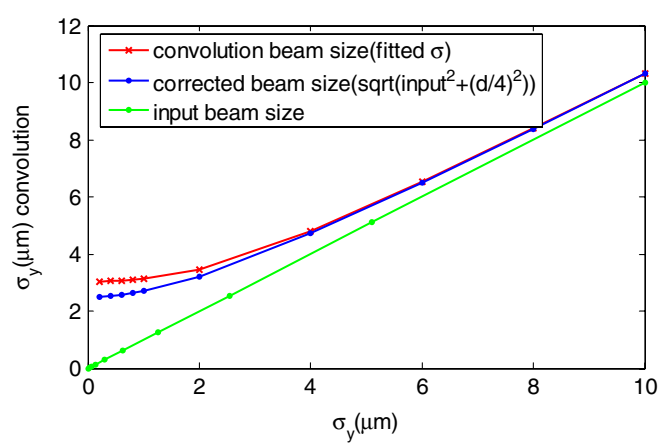

FIG. 2. Effect of folding a 10 μm diameter cylindrical wire with a Gaussian beam distribution as a function of its root mean square.

of using the tungsten wire to measure beam sizes smaller than its diameter. For beam sizes comparable or larger than about half the width of the wire, a good approximation is provided by just adding $d/4$, the second moment of the cylindrical wire distribution, in quadrature to the root mean square size of the beam particle distribution (see the blue curve in Fig. 2).

For smaller beam sizes, this approximation slightly underestimates the effect of the wire size. The error resulting from using it to correct measured distributions is however less than 7% for beam sizes larger than 2.5 μm. This bias is considered in the following sections.

III. DISPERSION AND BEAM SIZE MEASUREMENTS

In May 2009, the horizontal and vertical beam distributions were measured systematically using the post-IP tungsten wires, for a range of values of the damping ring rf frequency and of the current of QD0, the defocusing quadrupole magnet of the final doublet just before the IP. This enabled estimating the residual dispersion, the Twiss parameters, and the horizontal emittance.

A. Horizontal and vertical dispersion measurements

The results of horizontal and vertical dispersion measurements done at the post-IP wire scanners during the May 20 and May 28 shifts are displayed in Figs. 3 and 4 for three values of the QD0 quadrupole magnet current.

Each measurement involved recording the horizontal and vertical position shifts $\Delta x, y$ of the wire scanner signal distributions for different settings of the damping ring rf frequency and fitting linear dependencies to the data to extract the dispersions:

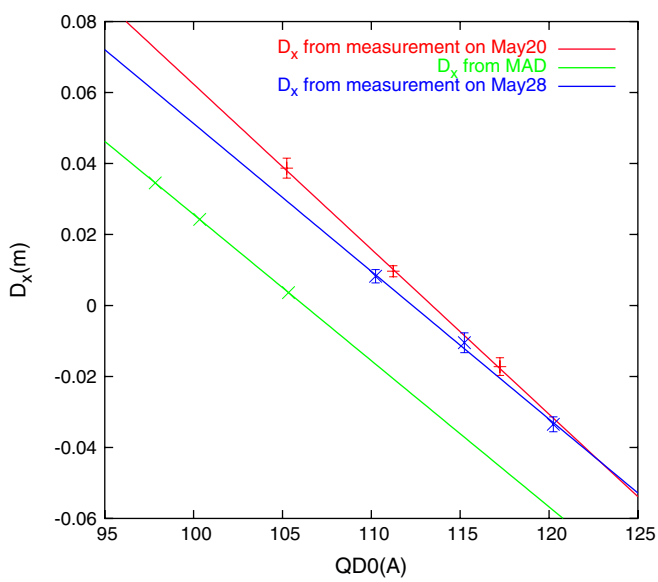

FIG. 3. Horizontal dispersion measurements at post-IP wire scanner and prediction from MAD.

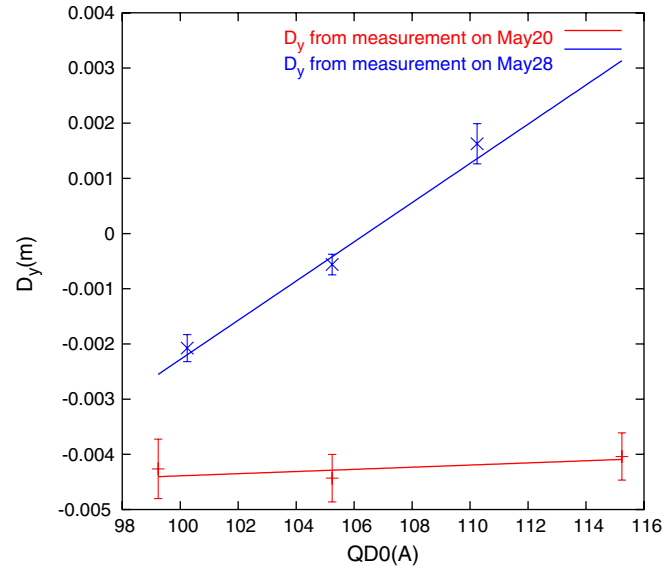

FIG. 4. Vertical dispersion measurements at post-IP wire scanner.

$$D_{x,y} = \frac{\Delta x, y}{\Delta p/p} \tag{3}$$

in which $\Delta p/p$ is the fractional momentum shift, related to the frequency change via

$$\frac{\Delta f}{f}\frac{1}{\alpha} = \frac{\Delta p}{p}, \tag{4}$$

where $\alpha = 0.002$ is the ATF ring momentum compaction factor and $f = 714$ MHz its frequency.

For each of the rf frequencies, the Gaussian peak of the bremsstrahlung distribution was measured 3 times and the averages were used. The error bars shown in Figs. 3 and 4 result from propagating the errors from the linear fits of positions with respect to rf frequency.

While there should not be any vertical dispersion near the IP in a perfect system, horizontal angular dispersion is an integral part of the design of the local chromaticity correction [5]. The values computed from the MAD optics simulation are shown for comparison in Fig. 3. The nominal value of the QD0 quadrupole magnet to shift both beam waists to the post-IP wire scanner is 105.24 A. As can be seen, significant anomalous horizontal spatial and vertical dispersion were measured in both shifts.

B. Horizontal and vertical waist scans

The beam sizes measured at the post-IP wire scanners during the May 20 and May 28 shifts are displayed in Table II as a function of the QD0 quadrupole magnet current.

The measured beam sizes include contributions from the dispersion and finite wire size, according to

TABLE II. Horizontal and vertical beam sizes measured with post-IP wire scanner without and with correction for wire size and dispersion. The uncorrected beam size errors are statistical uncertainties from fitting Gaussians to the bremsstrahlung photon distributions, while the corrected beam size errors include also uncertainties from the wire size and dispersion subtraction.

	Measurements on May 20				Measurements on May 28			
QD0, A	X, μm	X cor, μm	Y, μm	Y cor, μm	X, μm	X cor, μm	Y, μm	Y cor, μm
95.24							10.4 ± 0.1	9.5 ± 0.2
97.24			14.5 ± 0.3	13.9 ± 0.3				
100.24							7.2 ± 0.1	6.5 ± 0.1
101.24			8.9 ± 0.1	7.8 ± 0.1				
102.74							5.4 ± 0.1	4.7 ± 0.1
103.24			6.6 ± 0.2	5.1 ± 0.3				
105.24	36.2 ± 0.8	18.6 ± 2.1	4.9 ± 0.0	2.5 ± 0.1	44.5 ± 0.8	38.5 ± 1.3	3.8 ± 0.1	2.8 ± 0.1
107.24	31.0 ± 0.7	23.6 ± 1.1	5.8 ± 0.1	4.0 ± 0.2				
107.74					33.7 ± 0.6	30.6 ± 0.9	4.3 ± 0.1	3.5 ± 0.1
109.24	24.3 ± 0.4	20.7 ± 0.6	6.6 ± 0.1	5.1 ± 0.1				
110.24					25.4 ± 0.6	24.7 ± 0.6	5.1 ± 0.1	4.3 ± 0.1
111.24	14.1 ± 0.2	11.5 ± 0.4	7.7 ± 0.1	6.4 ± 0.1				
112.74					18.9 ± 0.4	18.5 ± 0.4	6.8 ± 0.1	6.0 ± 0.2
113.24	16.2 ± 0.3	15.8 ± 0.3						
115.24	26.6 ± 1.3	24.5 ± 1.4	13.1 ± 0.1	12.4 ± 0.1	16.8 ± 0.4	12.1 ± 0.9	7.5 ± 0.1	6.5 ± 0.2
117.74					23.7 ± 0.4	12.8 ± 1.6		
119.24			21.1 ± 0.2	20.7 ± 0.2				
120.24					33.7 ± 0.9	18.3 ± 2.4	12.2 ± 0.1	11.2 ± 0.3
122.74					47.5 ± 2.0	30.2 ± 3.6		
125.24					54.0 ± 1.5	29.8 ± 3.8		

$$\sigma_{x,y}{}^2 = \sigma_{x,y\,\mathrm{measured}}{}^2 - \left(\frac{\sigma_E}{E}\right)^2 D_{x,y}{}^2 - \left(\frac{d}{4}\right)^2, \qquad (5)$$

where $\sigma_E/E = 0.0008$ is the fractional energy spread and $d = 10$ μm the wire diameter. These contributions needed to be subtracted before interpreting in terms of Twiss parameters. The errors in the dispersion measurement and the uncertainty in the subtraction of the finite wire size (see Sec. II) were also propagated in the computation of the corrected beam sizes shown in Table II.

IV. TWISS PARAMETER ESTIMATION

A. Parametrization of beam sizes around the IP and post-IP waists

As explained in Sec. I, the square of the beam size in the vicinity of the IP or post-IP has a parabolic dependence with the longitudinal waist displacements $\Delta f_{x,y}$, see Eq. (1). For small variations $\Delta\mathcal{Q}$ of the QD0 quadrupole magnet integrated strength, Eq. (1) can be approximated by

$$\sigma_{x,y}{}^2 = \varepsilon_{x,y}\beta_{x,y} + \frac{\varepsilon_{x,y}}{\beta_{x,y}}(\Delta\mathcal{Q}\cdot a_{x,y})^2, \qquad (6)$$

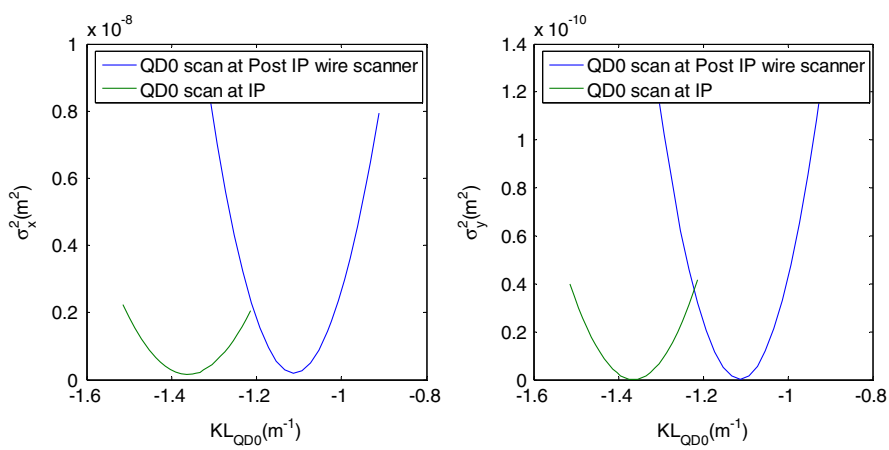

FIG. 5. Simulated beam size squared with respect to QD0 strength in the $\beta_{x/y} = 0.08/0.01$ m ATF2 optics, when focusing the beam to a waist at the IP (green curves) or post-IP (blue curve) locations.

TABLE III. Results of fitting parabolas to the squares of the horizontal and vertical beam sizes.

	$A[m^4]$	$B[m^{-1}]$	$C[m^2]$	$\mathrm{Cov}(A, C)$
May 20 X	$(2.97 \pm 0.94) \times 10^{-7}$	1.154 ± 0.003	$(1.49 \pm 0.38) \times 10^{-10}$	-0.605
May 20 Y	$(1.97 \pm 0.18) \times 10^{-8}$	1.102 ± 0.003	$(4.96 \pm 3.57) \times 10^{-12}$	-0.502
May 28 X	$(9.64 \pm 0.91) \times 10^{-8}$	1.208 ± 0.004	$(1.61 \pm 0.22) \times 10^{-10}$	0.161
May 28 Y	$(5.92 \pm 0.49) \times 10^{-9}$	1.106 ± 0.003	$(9.80 \pm 1.57) \times 10^{-12}$	-0.495

where $a_{x,y}$ are constants determined from the optical lattice using simulation.[1] These parameters are directly related to the focal length of the QD0 quadrupole magnet. They do not depend on the distortions of the incoming beam phase space. When QD0 is set to focus the beam to a waist at the post-IP wire scanner where the measurements presented in this paper are done, $a_{x,y} = 3.43, 2.23$ square meters.[2] The variations of the beam sizes with QD0 strength are shown for illustration in Fig. 5 from the simulation, when setting the optics to focus the beam to a waist at either the IP or the post-IP locations.

B. Estimation of Twiss parameters and of horizontal emittance

Using the corrected beam sizes in Table II, parabolas of form $\sigma^2(KL_{\mathrm{QD0}}) = A(KL_{\mathrm{QD0}} - B)^2 + C$ were fitted to the data taking into account the measurement errors, using the GNUPLOT software. The results are displayed in Table III and in Figs. 6 and 7, where the blue and red lines correspond, respectively, to the data corrected only for the wire size or corrected for both the wire size and dispersion.

Two methods were used to estimate the Twiss parameters and emittance from the parameters of these parabolas.

The first method, referred to as *method 1*, consists in evaluating the β parameter at the waist from the angular divergence contribution in the second term on the right-hand side of Eq. (6), using as input the emittance measured upstream, e.g., in the ATF2 diagnostic section (using methods described in [15]) or in the damping ring [16]. Equating the parabolic form fitted to the data with Eq. (6) then yields

$$\sigma^2 = \varepsilon_{\mathrm{EXT}}\beta(1 + a^2\Delta Q^2/\beta^2) = A(KL_{\mathrm{QD0}} - B)^2 + C$$
$$= A\Delta Q^2 + C.$$

One gets

$$A = \varepsilon_{\mathrm{EXT}} a^2/\beta \qquad \beta = \varepsilon_{\mathrm{EXT}} a^2/A, \tag{7}$$

where $\varepsilon_{\mathrm{EXT}}$ is the emittance used as input based on upstream measurements.

The second method, referred to as *method 2*, exploits the full information in the parabolic fit to infer both the β parameter and the emittance at the waist, by equating

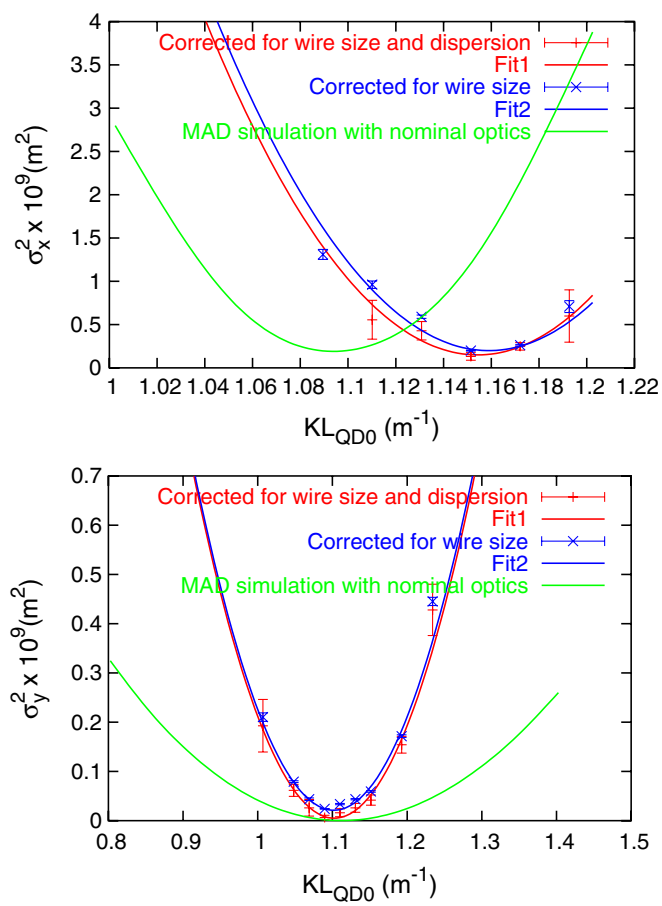

FIG. 6. Squares of horizontal and vertical beam sizes as a function of QD0 magnet strength on May 20 compared to the predictions from the optics simulation for the design large β optics. KL_{QD0} are the integrated QD0 magnet strengths, which are computed from the power supply currents using relations based on the magnetic measurement data [14].

[1]Variations in $\beta_{x,y}$ as the integrated strength of the QD0 quadrupole magnet is changed, of order $\Delta f_{x,y}/L^* \sim \beta_{x,y}/L^*$, where $L^* = 1$ meter is the distance between the exit of the final doublet and the IP, are neglected in (6). The induced biases, amounting to less than a few per mil in the nominal β optics and a few percent in the present large β configuration, are neglected in the following.

[2]For the nominal QD0 setting corresponding to a waist at the IP location, $a_{x,y} = 1.92, 1.23$.

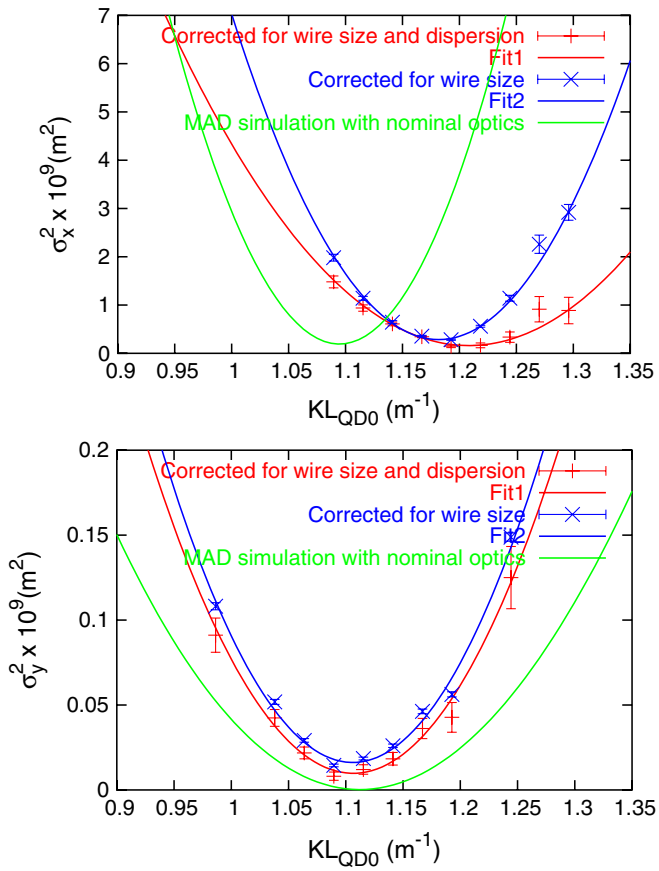

FIG. 7. Squares of horizontal and vertical beam sizes as a function of QD0 magnet strength on May 28 compared to the predictions from the optics simulation for the design large β optics. KL_{QD0} are the integrated QD0 magnet strengths, which are computed from the power supply currents using relations based on the magnetic measurement data [14].

$$A = \varepsilon a^2/\beta \qquad C = \varepsilon\beta. \tag{8}$$

One gets

$$\varepsilon = a^{-1}\sqrt{AC} \qquad \beta = a\sqrt{\frac{C}{A}}. \tag{9}$$

It should be noted that *method 2* is affected by large biases when the minimum of the parabola is smaller than the instrumental resolution, as is the case in the vertical plane, or when it includes significant residual optical aberrations, such as residual dispersion, cross-plane coupling effects, or chromaticity. This method was therefore only used to analyze parameters in the horizontal plane, while *method 1* could be used for both sets of measurements.

It is important in both methods to include measurements far enough on both sides of the minimum of the parabola, such that the quadratic term in Eq. (6) is well fitted. In practice, beam sizes at least 2 or 3 times the minimum are sufficient.

The horizontal and vertical Twiss parameters and the horizontal emittance obtained applying both methods to the data collected on May 20 and 28 are listed in Table IV. The horizontal and vertical emittances used as inputs for *method 1* were 1.86 nm and 20 pm for the data collected on May 20, and 1.7 nm and 11.5 pm for those collected on May 28, based on measurements in the diagnostic section earlier in each of the two shifts.

C. Discussion

The consistency of the results from *methods 1* and 2 was good for the horizontal emittance and β function using the data set from May 20 and agreed reasonably well with the nominal values. The results using the data set on May 28 showed discrepancies at the 50% level, indicating that input matching conditions of the beam had probably changed.

On the other hand, in both data sets the dispersion (see Fig. 3) and α_x Twiss parameter were mismatched in similar ways, and the estimated vertical β functions were also distorted.

Since these first measurements were performed before implementing optical corrections systematically, uncertainties in the input emittances used in *method 1* could not be properly accounted for. The beam intensity during the data taking on May 20 and 28 was recorded to be about 4×10^9 particles per bunch. For such intensities, the expected horizontal emittance is about 1.4 nm [17]. Using this value rather than that which was measured in the diagnostic section on May 28 (1.7 nm) would yield a somewhat improved agreement. Similarly, for the vertical β function, using the vertical emittance measured in the diagnostic section as input to *method 1* probably lead to an

TABLE IV. Twiss parameters and horizontal emittance computed from post-IP wire scanner measurements, compared with nominal values. The listed uncertainties result from propagating the errors in Eq. (6), taking into account the measured beam size statistical fit errors in Table III, the measured dispersion errors and a 7% uncertainty from the finite wire size correction.

		ε_x [m rad]	β_x [m]	α_x	ε_y[m rad]	β_y [m]	α_y
Nominal values		2.0×10^{-9}	0.099	0	1.2×10^{-11}	0.018	0
May 20	Method 1	1.86×10^{-9}	0.074 ± 0.023	-2.40	2×10^{-11}	0.0051 ± 0.0001	-0.205
	Method 2	$(1.94 \pm 0.25) \times 10^{-9}$	0.076 ± 0.019	-2.40			
May 28	Method 1	1.7×10^{-9}	0.21 ± 0.02	-1.744	1.15×10^{-11}	0.0096 ± 0.0001	0.816
	Method 2	$(1.15 \pm 0.10) \times 10^{-9}$	0.14 ± 0.01	-1.744			

underestimation as cross-plane coupling or dispersion effects were not fully corrected in those measurements.

In an attempt to explain the principal mismatches observed in the May 20 and May 28 data sets—for the horizontal dispersion and α_x Twiss parameter—a set of orthogonal knobs defined for D_x and $\alpha_{x,y}$ [18] using the QD0 and QF1 final doublet magnets and QF9, a focusing quadrupole located at a high dispersion point in the upstream part of the chromatic correction section of the final focus section, were used to simulate a correction. It was found that correction could easily be achieved with these knobs, with similar settings in both weeks, implying perhaps some systematic error in the magnetic transport. Trying to reproduce the measured $\alpha_{x,y}$ Twiss parameters with QD0 and QF1 alone, without using QF9, resulted in values for the horizontal dispersion which were not compatible with the observed ones, indicating that the error that would explain the behavior was not confined to the final doublet magnets.

A set of six matching quadrupole magnets located upstream of the final focus section, intended as part of the β matching procedure of the beam into the final focus section, were also tried to simulate a simultaneous correction of both waist shifts and of the mismatch in β_x and β_y at the IP. The resulting values for these six quadrupole magnets were all found to be within their operational ranges. They were a bit different in each shift, which showed that the betatron matching from the damping ring probably had changed.

V. CONCLUSIONS AND PROSPECTS

First ATF2 beam waist measurements were reported using the post-IP tungsten wire scanner, including the procedures to deal with dispersion and the finite size of the wire. Two methods to estimate the Twiss parameters from such measurements were described. When emittance values measured upstream in the system could be used as input, the angular divergence inferred from the waist scan could be used to estimate the value of the β function at the waist, without requiring the minimum beam size to be resolved. In the horizontal plane where the minimum beam size was large enough to be resolved, the emittance and β function could both be inferred from the waist scan.

Such procedures were applied to the first complete set of data collected in May 2009 and allowed checking the betatron phase space parameters near the IP, in order to quantify the level of mismatch and help prepare the beam before measurements with the Shintake monitor. The discrepancies which were found had magnitudes which could be corrected by standard procedures in the ATF2 beam line and in the damping ring.

During the on-going commissioning and operation of ATF2, measurements using the methods described in this paper are pursued systematically. Improved methods to estimate and subtract the residual dispersion and more comprehensive cross-plane coupling corrections are underway, as well as improvements to the acquisition and on-line modeling software expected to speed up the measurements and enable *in situ* analyses. This will allow checking the consistency with upstream measurements, identify any large error in the magnetic transport of the final focus beam line, and determine the most reliable data to be used as input to rematch the optics at the IP.

ACKNOWLEDGMENTS

This work is supported by the Agence Nationale de la Recherche of the French Ministry of Research (Programme Blanc, Projects No. ATF2-IN2P3-KEK and No. ANR-06-BLAN-0027) and by the National Natural Science Foundation of China (NSFC, Contracts No. 10775154 and No. 10525525). One of us (S. B.) would like to thank T. Tauchi, J. Urakawa, and K. Yokoya for being hosted at KEK during extended periods in 2009 to work on the ATF2 commissioning.

[1] ATF2 Proposal, SLAC R771, 2005.
[2] P. Bambade *et al.*, Phys. Rev. ST Accel. Beams **13**, 042801 (2010).
[3] ILC RDR, Report No. ILC-REPORT-2007-001 [http://www.linearcollider.org/].
[4] R. Tomàs, Phys. Rev. ST Accel. Beams **13**, 014801 (2010) [http://clic-study.web.cern.ch/clic-study/].
[5] P. Raimondi and A. Seryi, Phys. Rev. Lett. **86**, 3779 (2001).
[6] T. Shintake, Nucl. Instrum. Methods Phys. Res., Sect. A **311**, 453 (1992).
[7] T. Yamanaka *et al.*, IEEE NSS08 Conference Record 3308 (2008).
[8] S. Bai *et al.*, ATF-Report No. 08-05, 2008.
[9] H. Wiedemann, *Particle Accelerator Physics* (Springer, Berlin, 1999).
[10] C. Field, Report No. SLAC-PUB-6717, 1994.
[11] D. M. Cormick, "Fiber Loss Monitor and Carbon IP Scanner", setup and operational tips, 2008 [http://ilcagenda.linearcollider.org/getFile.py/access?contribId=7&sessionId=2&resId=1&materialId=slides&confId=3003].
[12] H. Hayano, ATF Report No. 00-22, 2002.
[13] Q. King, Report No. SPS-ABM-TM/Note/8802, 1988.
[14] C. Spencer *et al.*, at the 21st International Conference on Magnet Technology, 2009 [IEEE Trans. Appl. Supercond. (to be published)].
[15] I. Agapov, G. A. Blair, and M. Woodley, Phys. Rev. ST Accel. Beams **10**, 112801 (2007).
[16] K. Kubo *et al.*, in Proceedings of the 23rd Particle Accelerator Conference, Vancouver, Canada, 2009 (IEEE, Piscataway, NJ, 2009), FR1RAC05.
[17] Y. Honda *et al.*, Phys. Rev. Lett. **92**, 054802 (2004).
[18] B. Bolzon *et al.*, in The 1st International Particle Accelerator Conference, Kyoto, Japan, 2010 [http://ipac10.org/], THPD077.